International Journal of Thermal Sciences 128 (2018) 38–48

Contents lists available at ScienceDirect

International Journal of Thermal Sciences

journal homepage: www.elsevier.com/locate/ijts

Optimization-based design of easy-to-make devices for heat flux manipulation

Víctor D. Fachinotti[a,*], Ángel A. Ciarbonetti[a], Ignacio Peralta[a], Ignacio Rintoul[b]

[a] Centro de Investigación de Métodos Computacionales (CIMEC), Universidad Nacional del Litoral (UNL)/ Consejo Nacional de Investigaciones Científicas y Técnicas (CONICET), Predio CONICET "Dr. Alberto Cassano", Colectora Ruta Nac. 168 km 0, Paraje El Pozo, CP 3000, Santa Fe, Argentina

[b] Instituto de Desarrollo Tecnológico para la Industria Química (INTEC), Universidad Nacional del Litoral (UNL)/ Consejo Nacional de Investigaciones Científicas y Técnicas (CONICET), Predio CONICET "Dr. Alberto Cassano", Colectora Ruta Nac. 168 km 0, Paraje El Pozo, CP 3000, Santa Fe, Argentina

ARTICLE INFO

Keywords:
Heat flux manipulation
Optimization-based design
Easy-to-make device
Heat flux inversion
Metamaterial

ABSTRACT

In this work, we present a new method for the design of heat flux manipulating devices, with emphasis on their manufacturability. The design is obtained as solution of a nonlinear optimization problem where the objective function represents the given heat flux manipulation task, and the design variables define the material distribution in the device. In order to facilitate the fabrication of the device, the material at a given point is chosen between two materials with highly different conductivity. By this way, the whole device can be seen, in the large scale, as a metamaterial having a specific anisotropic effective conductivity. As an application example, we designed a heat flux inverter which was so simple that it could be hand-made. The performance of this device for heat flux inversion was experimentally tested, proving that it was more efficient than a more complex device designed using the classical transformation thermodynamics approach.

1. Introduction

Considering the major innovations enabled by the control of electromagnetic flux in electronics and communications [1] together with the analogies between electromagnetism and thermodynamics [2], the manipulation of heat flux is expected to lead to remarkable progress in thermodynamic applications. For instance, Chen and Lei [3] envisaged a dramatic enhancement of solar thermal collectors by using engineered thermal materials to concentrate the thermal flux.

These engineered materials are called metamaterials for having effective properties that goes *beyond* (*meta* in Greek) those found in nature, for instance negative apparent thermal conductivity [4]. In order to control heat conduction, a metamaterial must have a prescribed, spatially variable and generally anisotropic thermal conductivity. A device for heat flux manipulation consists of a body made of inhomogeneous metamaterial, which then has an inhomogeneous thermal conductivity distribution. In the literature, there are examples of devices designed and/or fabricated using metamaterials for different heat flux manipulation tasks: inversion [5–7], shielding [5–8], concentration [3,5–7], and cloaking [5,9]. Further, in our previous work, we designed metamaterial devices for combined shielding and cloaking [10] and combined concentration and cloaking [11]. In all these cases, the device serves to manipulate the heat flux in a given, say academic, way. Of course, they were effective to prove the efficiency and the potential of metamaterials, but their practical application needs further research and development.

We identify two main obstacles to the extension of the practical use of metamaterials. First, the classical approach for metamaterial design, that used in Refs. [3,5,8,9], is based on the thermodynamic transformation concept inherited from electromagnetism [12]. This methodology is, if not impossible, difficult to apply to general cases, for instance: 1) when either the metamaterial device or the region where it is embedded is not geometrically simple; 2) when the heat flux must be manipulated in general ways, or 3) when the external heat flux is not homogeneous.

To deal with arbitrary domains and boundary conditions, Dede [13] formulated the problem of metamaterial design as an optimization problem whose solution gives the metamaterial distribution. By this way, Dede determined the spatial variation of the orientation of the inclusions in a composite plate in order to minimize the thermal resistance of the plate. Later, Dede et al. [7] determined the orientation distribution in devices for heat inversion, concentration or shielding in a given portion of a plate. They represented each one of these tasks using a different objective function.

In our previous works [10,11], we have applied the optimization-based methodology for the design of thermal metamaterials for

* Corresponding author.
E-mail address: vfachino@intec.unl.edu.ar (V.D. Fachinotti).

https://doi.org/10.1016/j.ijthermalsci.2018.02.009
Received 6 April 2017; Received in revised form 7 February 2018; Accepted 8 February 2018

shielding and concentration (in both cases, combined with cloaking), respectively. We chose as thermal metamaterial a laminate of materials with high conductivity contrast, and we considered not only the orientation of the laminate but also the relative thickness of the layers at each finite element inside the device as design variables. Unlike Dede et al. [7], we defined a unique objective function for general manipulation tasks, capable of representing shielding, concentration, inversion and cloaking (as well as combination of these tasks) as particular cases. By this way, any so-defined heat manipulation task gives rise to a mathematically identical optimization problem. This general approach also serves for the purposes of this paper.

The other obstacle for real-life applications is the difficult fabrication of the metamaterial device, mainly because it has to be made with a precise inhomogeneous metamaterial distribution. This was circumvented by Vemuri et al. [14] by fabricating a device for heat concentration and cloaking using a homogeneous laminate that was arranged in two different orientations at each fourth of the device. By this way, they approached as well as possible (actually, quite poorly) the thermal conductivity distribution required to accomplish the given tasks.

So, the main goal of this paper is the design of easy-to-make devices for heat flux manipulation. Here, we postulate that the easiest-to-make device is that resembling a metamaterial only at the macroscale (that of the whole device) but is made of pure materials at the microscale. Specifically, at a given finite element in the device, a choice is made between two materials having sensibly different thermal conductivity. Further, this conductivity is not necessarily anisotropic as it is compulsory for guiding the heat flux using inhomogeneous metamaterials.

Like in our previous work using metamaterials [10,11], the desired heat flux manipulation task constitutes the objective function of a nonlinear constrained optimization problem, where the design variables define the material distribution throughout the heat flux manipulating device. Since the material at a finite element is either of two materials, the current problem strongly resembles a structural topology optimization problems [15]. Applications of topology optimization can also be found for heat conduction [16,17]. However, the current problem has crucial differences with classical topology optimization problems. First, the objective function in topology optimization is either the material volume or the compliance [15], linearly dependent on the design or the state variables, respectively. Meanwhile, the current objective represents the given task and is a highly nonlinear function of the design and the state variables. Secondly, to consider the material volume (either as an objective or as a constraint) is imperative for topology optimization but not for heat flux manipulation. Actually, we are purely concerned by the accomplishment of the task, obviating (at least, within the scope of this work) the minimization of material volume or the uniqueness of the solution.

Finally, we applied this optimization-based method to the design of a device for heat flux inversion. This is an extreme heat flux guidance problem, any other desired direction for the heat flux being an intermediate case. The so-designed device was so simple that we were able to hand-made it. We test this device for the experimental assessment of its efficiency, which was found to be better than that of Narayana and Sato's device [5], a considerable more complex device, designed on the base of the classical transformation thermodynamics approach and usually taken as reference to highlight the potential of metamaterials [1,2].

2. Heat conduction in a heterogeneous body

Let us consider the domain Ω in Fig. 1, made of a heterogeneous material, with boundary $\partial\Omega$ divided in two non-overlapping portions: $\partial\Omega_q$ (where the heat flux q_{wall} is prescribed) and $\partial\Omega_T$ (where the temperature T_{wall} is prescribed). In steady state, the heat conduction in Ω is governed by the equation

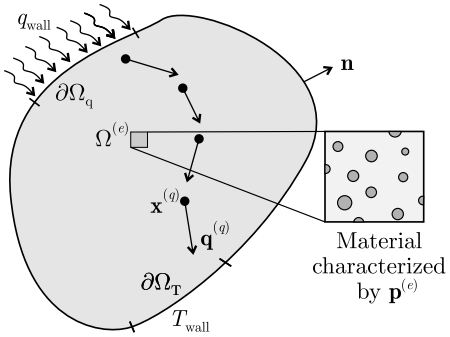

Fig. 1. Heat flux manipulation problem in the domain Ω where the effective properties at each sub-domain $\Omega^{(e)}$ depend on a set of parameters $\mathbf{p}^{(e)}$.

$$\operatorname{div}(\mathbf{q}) = s \quad \text{in } \Omega, \tag{1}$$

and the boundary conditions:

$$T = T_{wall} \quad \text{in } \partial\Omega_T, \tag{2}$$

$$\mathbf{q}\cdot\mathbf{n} = q_{wall} \quad \text{in } \partial\Omega_q, \tag{3}$$

where $\mathbf{q}$ is the heat flux vector field, s is the internal heat source, T is the temperature, and $\mathbf{n}$ is the unit vector normal to and pointing outwards $\partial\Omega$.

Assuming that the heat flux obeys the Fourier law, it is given by:

$$\mathbf{q} = -\mathbf{k}\,\operatorname{grad} T, \tag{4}$$

where $\mathbf{k}$ is the effective thermal conductivity, a second-order tensor.

Using the finite element method (FEM), the temperature field in Ω is approximated as follows:

$$T(\mathbf{x}) = N_j(\mathbf{x})T_j = \mathbf{N}(\mathbf{x})\cdot\mathbf{T} \quad \forall\, \mathbf{x} \in \Omega, \tag{5}$$

where N_j is shape function associated to the node j of the finite element mesh representing Ω, and T_j is the (unknown) temperature at this node. In the standard (Galerkin) FEM, the nodal temperature vector $\mathbf{T}$ is the solution of the algebraic system of equations

$$\mathbf{KT} = \mathbf{F}, \tag{6}$$

where $\mathbf{K}$ and $\mathbf{F}$ are the global conductivity matrix and the nodal heat flux vector, respectively, given by

$$\mathbf{K} = \int_\Omega \mathbf{B}^T\mathbf{k}\mathbf{B}\,\mathrm{d}V, \tag{7}$$

$$\mathbf{F} = \int_\Omega s\mathbf{N}\,\mathrm{d}V + \int_{\partial\Omega_q} q_{wall}\mathbf{N}\,\mathrm{d}S, \tag{8}$$

with $B_{ij} = \partial N_j/\partial x_i$, such that $\mathbf{BT} = \operatorname{grad} T$.

The system of equation (6) is the FEM version of the heat conduction (1), subject to the boundary conditions (2) and (3), for the heat flux obeying the Fourier law (4). This is a classical FEM problem, whose details can be found for instance in the book of Zienkiewicz and Taylor of the basics of FEM [18].

Let us asume that Ω is a heterogeneous body. Specifically, the material is assumed to vary element-wise in the finite element mesh $\Omega = \Omega^{(1)} \cup \Omega^{(2)} \cup \ldots \cup \Omega^{(E)}$. At the finite element $\Omega^{(e)}$, the effective or material properties are functions of a finite number of parameters grouped in the vector $\mathbf{p}^{(e)} = [p_1^{(e)}, p_2^{(e)}, \ldots, p_M^{(e)}]$, as shown in Fig. 1. Examples of such parameters are the fiber orientation in fiber-reinforced polymers [19], the density and irregularity factors in materials with isolated inhomogeneities [20,21], the size of particles or beads in coating of dental implants [22,23], and the density in topological optimization [24]. So, the effective conductivity at the element $\Omega^{(e)}$ is

$$\mathbf{k}^{(e)} = \mathbf{k}(\mathbf{p}^{(e)}). \tag{9}$$

Further, made of contributions from all the elements of the mesh, the global conductivity matrix $\mathbf{K}$ is then

$$\mathbf{K} = \mathbf{K}(\mathbf{P}) \tag{10}$$

with

$$\mathbf{P} = [\mathbf{p}^{(1)}\,\mathbf{p}^{(2)}\,...\,\mathbf{p}^{(E)}]. \tag{11}$$

Consequently, the nodal temperature $\mathbf{T}$ is a function of $\mathbf{P}$, and so it is the temperature field T in Ω.

3. The heat flux manipulation problem

The heat flux at the point $\mathbf{x}^{(q)}$ inside the finite element $\Omega^{(q)}$ is

$$\mathbf{q}^{(q)} = -\mathbf{k}(\mathbf{p}^{(q)})\mathbf{B}(\mathbf{x}^{(q)})\mathbf{T}(\mathbf{P}) \equiv \mathbf{q}^{(q)}(\mathbf{P}). \tag{12}$$

By manipulating the heat flux inside Ω, we mean to force the heat flux to take prescribed values $\overline{\mathbf{q}}^{(q)}$ at a series of checking points $\mathbf{x}^{(q)} \in \Omega$, with $\mathbf{x}^{(q)}$ located inside the finite element $\Omega^{(q)}$ and $q = 1,2, ...,Q$, see Fig. 1. To accomplish this task, we must find $\mathbf{P}$ (determining the entire material distribution in Ω) such that

$$\mathbf{q}^{(q)}(\mathbf{P}) = \overline{\mathbf{q}}^{(q)}, \quad \text{for } q = 1,2...,Q. \tag{13}$$

The search of $\mathbf{P}$ is constrained to an admissible design space $\mathscr{D}$. In general, it will not be possible to accomplish the given task for $\mathbf{P} \in \mathscr{D}$. Then, let us do that as well as possible by solving the following nonlinear constrained optimization problem:

$$\min_{\mathbf{P}\in\mathscr{D}} f_{\text{obj}}(\mathbf{P}), \tag{14}$$

where f_{obj} is the nonlinear objective function, which measures the global error in the accomplishment of the task at all the checking points, defined as

$$f_{\text{obj}}(\mathbf{P}) = \left[\sum_{q=1}^{Q} w^{(q)}\|\mathbf{q}^{(q)}(\mathbf{P}) - \overline{\mathbf{q}}^{(q)}\|^2\right]^{1/2}, \tag{15}$$

with $w^{(q)}$ denoting the weight allocated to the accomplishment of the task at $\mathbf{x}^{(q)}$, which satisfies $\sum_{q=1}^{Q} w^{(q)} = 1$. Note that this is a multi-objective optimization problem treated with the weighted-sum approach. Further, for $w^{(q)} = 1/Q = constant$, f_{obj} defines the root mean square error (RMSE) in the accomplishment of the task at all the checking points.

Prior to this work [11], we use composite materials with prescribed anisotropy ("metamaterials") to manipulate the heat flux. There, we did not consider manufacturability constraints but we recognized they were essential to allow the fabrication of pieces from these metamaterials. Now, we are particularly concerned by the manufacturability of computationally designed devices. However, instead of assuring it by means of additional constraints for the optimization problem [14], let us start by the simplest solution: the material at a finite element $\Omega^{(e)}$ can be one of two materials, having isotropic conductivities $k_{\min}$ and $k_{\max}$, with $k_{\max} \gg k_{\min}$. Then, following the SIMP (Solid Isotropic Material with Penalization) approach – classical to topological optimization [15] –, the conductivity at the element $\Omega^{(e)}$ is defined as:

$$k^{(e)} = k_{\min} + (\rho^{(e)})^p(k_{\max} - k_{\min}), \tag{16}$$

where $p > 1$, and $\rho^{(e)}$ is an artificial density, with $0 \le \rho^{(e)} \le 1$. By choosing $p \ge 3$, $(\rho^{(e)})^p$ is compelled to tend to either 0 or 1, i.e., the material at $\Omega^{(e)}$ is forced to be either that of conductivity $k_{\min}$ or that of conductivity $k_{\max}$, respectively, instead of a mixture of them. Note that, once $k_{\min}$ and $k_{\max}$ are given, the material at $\Omega^{(e)}$ is completely determined by only one parameter: $P_e \equiv p_1^{(e)} \equiv \rho^{(e)}$.

3.1. Sensitivity analysis

Crucial to the efficient solution of the nonlinear constrained optimization problem (14) is the analytical computation of the sensitivity of the objective function f_{obj} to the changes in the design variable $P_e = \rho^{(e)}$, given by $\partial f_{\text{obj}}/\partial P_e$. As suggested by Tortorelli and Michaleris [25] for computational efficiency, this derivative is computed using the adjoint method. To this end, the objective function f_{obj} is rewritten as

$$f_{\text{obj}}(\mathbf{P}) - \boldsymbol{\lambda}\cdot(\mathbf{K}\mathbf{T} - \mathbf{F}), \tag{17}$$

where the last term is null in virtue of the equilibrium equation (6), and $\boldsymbol{\lambda}$ is an arbitrary real vector (to be determined).

Differentiating equation (17) with respect to P_e, we obtain

$$\begin{aligned}\frac{\partial f_{\text{obj}}}{\partial P_e} &= \left.\frac{\partial f_{\text{obj}}}{\partial P_e}\right|_{\mathbf{T}=constant} + \frac{\partial f_{\text{obj}}}{\partial \mathbf{T}}\cdot\frac{\partial \mathbf{T}}{\partial P_e} - \boldsymbol{\lambda}\cdot\left(\frac{\partial \mathbf{K}}{\partial P_e}\mathbf{T} + \mathbf{K}\frac{\partial \mathbf{T}}{\partial P_e}\right)\\ &= \left.\frac{\partial f_{\text{obj}}}{\partial P_e}\right|_{\mathbf{T}=constant} - \boldsymbol{\lambda}\cdot\frac{\partial \mathbf{K}}{\partial P_e}\mathbf{T} - \left(\mathbf{K}\boldsymbol{\lambda} - \frac{\partial f_{\text{obj}}}{\partial \mathbf{T}}\right)\cdot\frac{\partial \mathbf{T}}{\partial P_e},\end{aligned} \tag{18}$$

where

$$\frac{\partial f_{\text{obj}}}{\partial \mathbf{T}} = -\frac{1}{f_{\text{obj}}}\sum_{q=1}^{Q} k^{(q)}w^{(q)}(\mathbf{q}^{(q)} - \overline{\mathbf{q}}^{(q)})\mathbf{B}(\mathbf{x}^{(q)}), \tag{19}$$

$$\left.\frac{\partial f_{\text{obj}}}{\partial P_e}\right|_{\mathbf{T}=constant} = -\frac{1}{f_{\text{obj}}}\sum_{q=1}^{Q}\frac{\partial k^{(q)}}{\partial P_e}w^{(q)}(\mathbf{q}^{(q)} - \overline{\mathbf{q}}^{(q)})\mathbf{B}(\mathbf{x}^{(q)})\mathbf{T}, \tag{20}$$

$$\frac{\partial \mathbf{K}}{\partial P_e} = \frac{\partial k^{(e)}}{\partial P_e}\int_{\Omega^{(e)}} \mathbf{B}^T\mathbf{B}\,dV. \tag{21}$$

Being $k^{(q)}$ the conductivity at the point $\mathbf{x}^{(q)} \in \Omega^{(q)}$ given by equation (16), its derivative with respect to the design variable P_e (equal to the artificial density at the element $\Omega^{(e)}$) is

$$\frac{\partial k^{(q)}}{\partial P_e} = \begin{cases} pP_e^{p-1}(k_{\max} - k_{\min}) & \text{if } \mathbf{x}^{(q)} \in \Omega^{(e)},\\ 0 & \text{otherwise.}\end{cases} \tag{22}$$

Note that if all the checking points $\mathbf{x}^{(q)}$ lie in elements with fixed density, the derivative given by equation (20) is null. Normally, we put only one checking point per finite element, so, even if the checking points lie in elements with unknown density, the sum in equation (20) has at most only one term.

Now, to avoid the expensive computation of $\partial\mathbf{T}/\partial P_e$ in equation (18), we adopt $\boldsymbol{\lambda}$ as solution of the following linear equation:

$$\mathbf{K}\boldsymbol{\lambda} - \frac{\partial f_{\text{obj}}}{\partial \mathbf{T}} = 0. \tag{23}$$

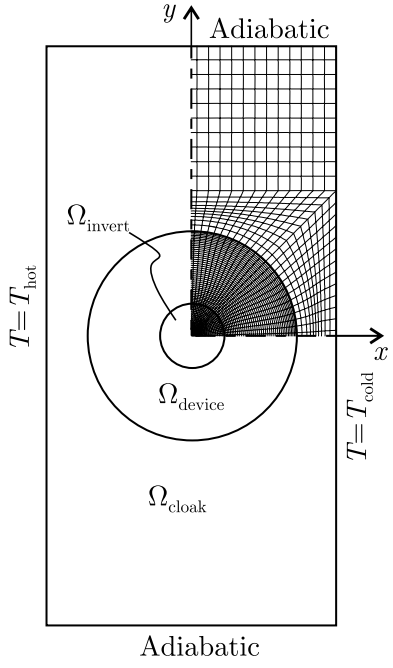

Fig. 2. Domain Ω, union of the region Ω_{device} occupied by the device, the region Ω_{invert} of heat flux inversion, and the region Ω_{cloak} of unaffected heat flux.

Finally, once such $\boldsymbol{\lambda}$ is determined, the sensitivity of the objective function to the change of the artificial density in the finite element $\Omega^{(e)}$ is

$$\frac{\partial f_{\text{obj}}}{\partial P_e} = \left.\frac{\partial f_{\text{obj}}}{\partial P_e}\right|_{\mathbf{T}=constant} - \boldsymbol{\lambda}\cdot\frac{\partial \mathbf{K}}{\partial P_e}\mathbf{T}. \tag{24}$$

4. Design of a heat flux inversion and cloaking device

Let us design a device for heat flux inversion and cloaking as alternative to that proposed by Narayana and Sato [5], who first determined the required distribution of anisotropic conductivity following the transformation-based methodology employed by Chen and Chan [26] to rotate electromagnetic waves, and then approached such distribution by using metamaterials made of alternating layers of copper and polyurethane.

Here, Ω denotes the region where the heat flux must be manipulated, a rectangle with sides $L_x = 9$ cm and $L_y = 18$ cm, subject to the following boundary conditions: $T = T_{\max} = 321.85$ K for $x = -L_x/2$, $T = T_{\min} = 283.15$ K for $x = L_x/2$, and $\mathbf{q}\cdot\mathbf{n} = 0$ for $y = \pm L_y/2$. So, the plate originally undergoes a homogeneous temperature gradient with magnitude 430 K/m and direction $-x$, identical to that found in the Narayana and Sato's heat flux inversion and cloaking problem [5]. Further, considering the plate full of agar water with isotropic thermal conductivity $k_{\text{agar}} = 0.57$ $\text{Wm}^{-1}\text{K}^{-1}$, the heat flux in the plate is given by the vector $\mathbf{q}_0$ with magnitude $q_0 = 245.10$ Wm^{-2} and direction x.

A device occupying the region Ω_{device} (a centered ring with inner diameter $d_{\text{inner}} = 2$ cm and outer diameter $d_{\text{outer}} = 6.5$ cm) will be designed to invert the heat flux in Ω_{invert} (inside the device) and keep the heat flux unaffected in Ω_{cloak} (outside the device). Fig. 2 shows the domain $\Omega = \Omega_{\text{device}} \cup \Omega_{\text{cloak}} \cup \Omega_{\text{invert}}$, the boundary conditions, and a quarter of the finite element mesh for Ω, which is symmetric with respect to the axes x and y. The whole mesh for Ω has 7625 bilinear finite elements, which are distributed as follows: $N_{\text{device}} = 4000$ elements in Ω_{device}, $N_{\text{invert}} = 2125$ elements in Ω_{invert}, and $N_{\text{cloak}} = 1500$ elements in Ω_{cloak}.

The device will be fabricated using copper and polymethyl methacrylate (PMMA), having conductivities $k_{\max} = 403$ $\text{Wm}^{-1}\text{K}^{-1}$ and $k_{\min} = 0.22$ $\text{Wm}^{-1}\text{K}^{-1}$, respectively. The thermal conduction

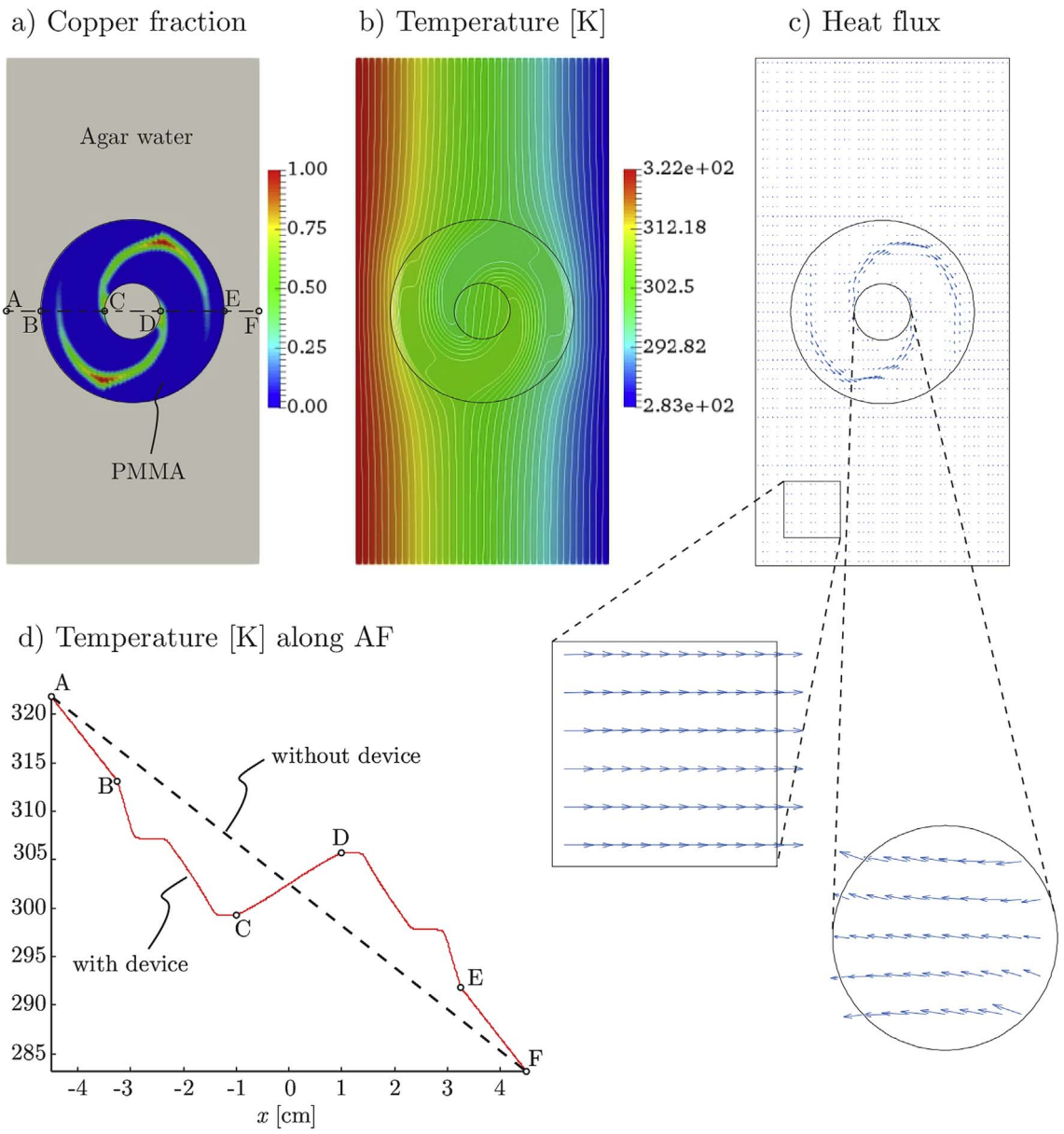

Fig. 3. Optimal solution for the heat flux inversion and cloaking device: a) Fraction of copper in the device; b) temperature in the plate, with isotherms separated by 0.9923 K; c) heat flux in the plate, with details of the heat flux inside and outside the device; d) temperature along the line AF.

properties of all the materials involved in this example, either in the device or in the plate, are those found in the Narayana and Sato's heat flux inversion and cloaking problem [5].

4.1. Material distribution in the device

For the current heat flux inversion and cloaking problem, the minimization problem is defined by equation (14) with the objective function given by equation (15), where $\mathbf{q}^{(q)} = -\mathbf{q}_0$ is prescribed for all the elements $\Omega^{(q)} \in \Omega_{\text{invert}}$ and $\mathbf{q}^{(q)} = \mathbf{q}_0$ is prescribed for all the elements $\Omega^{(q)} \in \Omega_{\text{cloak}}$ and $w^{(q)} = 1/Q$ (with $Q = N_{\text{invert}} + N_{\text{cloak}} = 3625$) is assumed to be constant, i.e.

$$f_{\text{obj}}(\mathbf{P}) = \left[\frac{1}{Q}\left(\sum_{q|\Omega^{(q)}\in\Omega_{\text{invert}}} \|\mathbf{q}^{(q)}(\mathbf{P}) + \mathbf{q}_0\|^2 + \sum_{q|\Omega^{(q)}\in\Omega_{\text{cloak}}} \|\mathbf{q}^{(q)}(\mathbf{P}) - \mathbf{q}_0\|^2\right)\right]^{1/2}. \tag{25}$$

This is the RMSE in the accomplishment of the inversion task at all the elements in Ω_{invert} combined with the cloaking task at all the elements in Ω_{cloak}. The design variables are the artificial densities P_e at the $N = 4000$ finite elements in Ω_{device}. Further, the minimization of the nonlinear function $f_{\text{obj}}(\mathbf{P})$ is subject to the box constraints $0 \le P_e \le 1$.

The solution of this optimization problem gives the vector $\mathbf{P}$ of design variables defining the material distribution throughout the device. Such device is a ring that induces the inversion of the enclosed region without disturbing the exterior heat flux; both tasks are accomplished, if not exactly, up to a minimum RMSE.

4.2. Density filtering

Usually, the so-computed material distribution is affected by "checkerboard"-type instabilities. This is a well-known and widely studied defect in material distribution problems (see the book of Bendsøe and Sigmund [15] and references therein), which can be avoided using the density filtering technique proposed by Sigmund

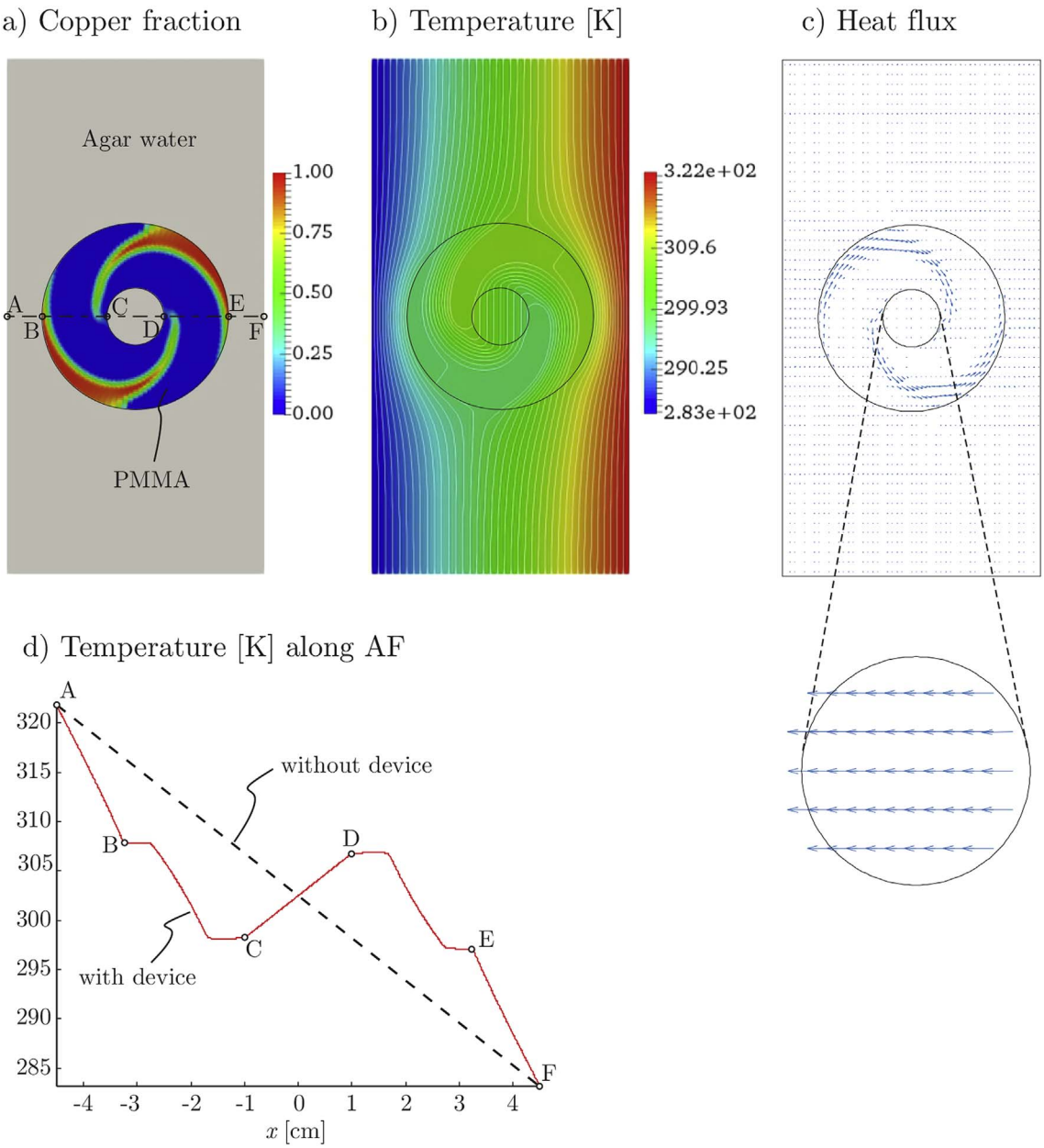

Fig. 4. Optimal solution for the heat flux inversion device: a) Fraction of copper in the device; b) temperature in the plate, with isotherms separated by 0.9923 K; c) heat flux in the plate, with a detail of the heat flux inside the device; d) temperature along the line AF.

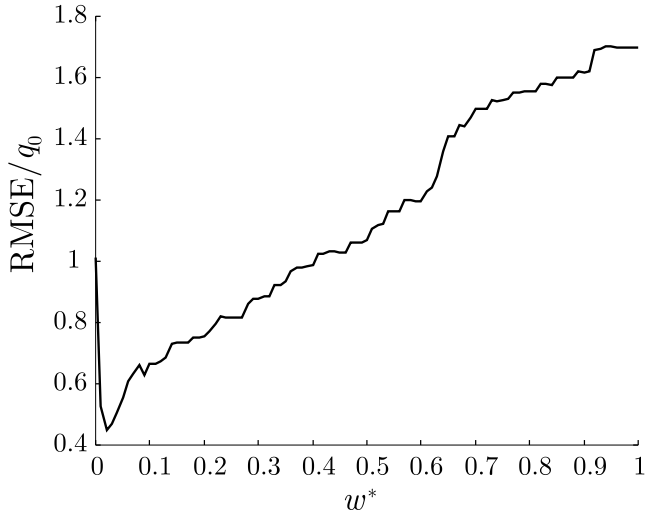

Fig. 5. Root mean square error for the heat inversion task as a function of the parameter w^* (the threshold above which the fraction of copper is assumed to be unity).

[24]. The design variable associated to the element $\Omega^{(e)}$ is still P_e, but the material in $\Omega^{(e)}$ is now determined by the filtered artificial density

$$\widetilde{P}_e = \frac{\sum_{i=1}^{N} \langle r_{\text{filtr}} - \Delta_{ei} \rangle P}{\sum_{i=1}^{N} \langle r_{\text{filtr}} - \Delta_{ei} \rangle}, \tag{26}$$

where r_{filtr} is the filter radius (to be adopted), P_i is the design variable associated to the finite element $\Omega^{(i)} \in \Omega_{\text{device}}$, Δ_{ei} is the distance between the centers of $\Omega^{(e)}$ and $\Omega^{(i)}$, and $\langle x \rangle$ is the ramp function ($\langle x \rangle = x$ for $x > 0$, and $\langle x \rangle = 0$ for $x \leq 0$), so that the sums in the above equation involve only those elements whose centers are at a distance not greater than r_{filtr} from the center of $\Omega^{(e)}$.

Note that the density filter (26) is linear, so that the relationship between the vector $\widetilde{\mathbf{P}}$ (whose e-th entry is the filtered density $\widetilde{P}_e$) and the design variables $\mathbf{P}$ can be expressed as

$$\widetilde{\mathbf{P}} = \mathbf{A}\mathbf{P}, \tag{27}$$

where $\mathbf{A}$ is the square matrix with entries

$$A_{ej} = \frac{\langle r_{\text{filtr}} - \Delta_{ej} \rangle}{\sum_{i=1}^{N} \langle r_{\text{filtr}} - \Delta_{ei} \rangle} \tag{28}$$

Since the material properties are now determined by $\widetilde{\mathbf{P}}$ instead of $\mathbf{P}$, the objective function f_{obj} must be replaced by

$$\widetilde{f}_{\text{obj}}(\mathbf{P}) = f_{\text{obj}}(\widetilde{\mathbf{P}}), \tag{29}$$

Consequently, the sensitivity of the objective function to changes in the design variables (that are still given by $\mathbf{P}$) is given by

$$\frac{\partial \widetilde{f}_{\text{obj}}(\mathbf{P})}{\partial P_e} = \frac{\partial f_{\text{obj}}(\widetilde{\mathbf{P}})}{\partial \widetilde{P}_i} A_{ie}. \tag{30}$$

where $\partial f_{\text{obj}}(\widetilde{\mathbf{P}})/\partial \widetilde{P}_i$ is defined by equation (24) by simply replacing $\mathbf{P}$ by $\widetilde{\mathbf{P}}$.

4.3. Solution of the optimization problem

So, considering density filtering, the nonlinear constrained optimization problem to be finally solved takes the form

$$\min_{\mathbf{P}} \widetilde{f}_{\text{obj}}(\mathbf{P}) \text{subject to } 0 \leq P_e \leq 1. \tag{31}$$

To this end, we use the interior point algorithm proposed by Wächter and Biegler [27], which is a primal-dual barrier method that deals with the box constraints by introducing slack variables and their corresponding Lagrange multipliers (dual variables). This algorithm is well-suited for large-scale optimization problems, and is implemented in the code IPOPT, freely downloadable from https://projects.coin-or.org/Ipopt. Here, we use IPOPT version 3.12.7.

Every time $\mathbf{P}$ is updated along the iteration process, IPOPT calls an external routine for the computation of the objective function $\widetilde{f}_{\text{obj}}$. Concerning the sensitivity vector (the so-called gradient in the IPOPT nomenclature) $\partial \widetilde{f}_{\text{obj}}/\partial \mathbf{P}$ (that whose e-th entry is $\partial \widetilde{f}_{\text{obj}}/\partial P_e$), IPOPT can compute it using numerical derivatives, but this is unaffordable in presence of a large number of design variables, as it the current case. So, we provided IPOPT with this gradient computed in the analytical way described in Section 3.1.

For the computation of $\widetilde{f}_{\text{obj}}$ and its gradient, we wrote dedicated routines in GNU Octave [28], a free software for scientific programming; these routines take $\mathbf{P}$ as input and give either the objective function or its gradient as output. Note that the evaluation of these functions involves a finite element analysis for the material distribution given by $\mathbf{P}$, which has also been coded in GNU Octave.

IPOPT should also be fed with the Hessian matrix, that whose components are the second derivatives of $\widetilde{f}_{\text{obj}}$. We let IPOPT approximate it using the limited-memory quasi-Newton method known as L-BFGS [29].

Further settings for the current heat flux manipulation problem are: $p = 3$ as the exponent of the SIMP power function (16) defining the effective conductivity (as typically suggested for material distribution problems [15]); $\tilde{r}_{\text{filtr}} = 3.5$ mm (i.e., four times the average element size in Ω_{device}) as the filtering radius in the equation (26) defining the density filtering; and $P_e = 0.5$ for all $e = 1,2...,N$ as initial guess.

4.4. Results and discussion

Fig. 3a shows the optimal solution for the copper fraction in the device, given at the element $\Omega^{(e)} \in \Omega_{\text{device}}$ by $w^{(e)}_{\text{copper}} = (\widetilde{P}_e)^p$, with $0 \leq w^{(e)}_{\text{copper}} \leq 1$; $w^{(e)}_{\text{copper}} = 0$ implies that the material in $\Omega^{(e)}$ is PMMA. Fig. 3b and c give the temperature and heat flux distributions in the plate as result of the inclusion of such device. Fig. 3d details the temperature along the line AF, where it is clearly appreciated how the temperature gradient is inverted in the segment CD.

Quantitatively, such device accomplishes the combined inversion and cloaking task with RMSE = $0.2788q_0$; individually, RMSE = $0.2287q_0$ for the inversion task in Ω_{invert}, and RMSE = $0.3372q_0$ for the cloaking task in Ω_{cloak}.

The fan-like structure observed Fig. 3a is also present in Narayana and Sato's device [5], but, while the current one has only two arms, these authors' had 96. Not only the device defined by Fig. 3a is simpler than that in Ref. [5] but it also better accomplishes the inversion task. The numerically computed heat flux is $\mathbf{q}^{(c)} = -0.56q_0[\cos 24^\circ \sin 24^\circ]^T q_0$ at the center of the device in Ref. [5], while it is $\mathbf{q}^{(c)} = -0.84q_0[\cos(-6^\circ) \sin(-6^\circ)]^T$ at the center of the current device. Regarding the cloaking task, the goodness of the device proposed by Narayana and Sato was not quantitatively assessed in their work [5].

5. Design of a heat flux inverter

Besides the goodness in accomplishing a given task, the above results prove another crucial advantage of the optimization-based approach for designing thermal manipulating devices with respect to the transformation-based approach used by Narayana and Sato [5]: Only the given specific task is accomplished. By this way, the current device is not “overdimensioned”: it has not 96 arms to invert the flux coming from anywhere but only two arms to invert the given flux.

If the desired task is only heat inversion, the cloaking task is a collateral result of using the transformation-based approach. Actually, we will demonstrate here that the inversion task can be better accomplished if the cloaking task is obviated.

The optimization problem is identical to that solved in the previous section, except that the terms from Ω_{cloak} in the objective function (25) are now excluded (and so, $Q = N_{\text{invert}} = 2125$). This problem is solved using

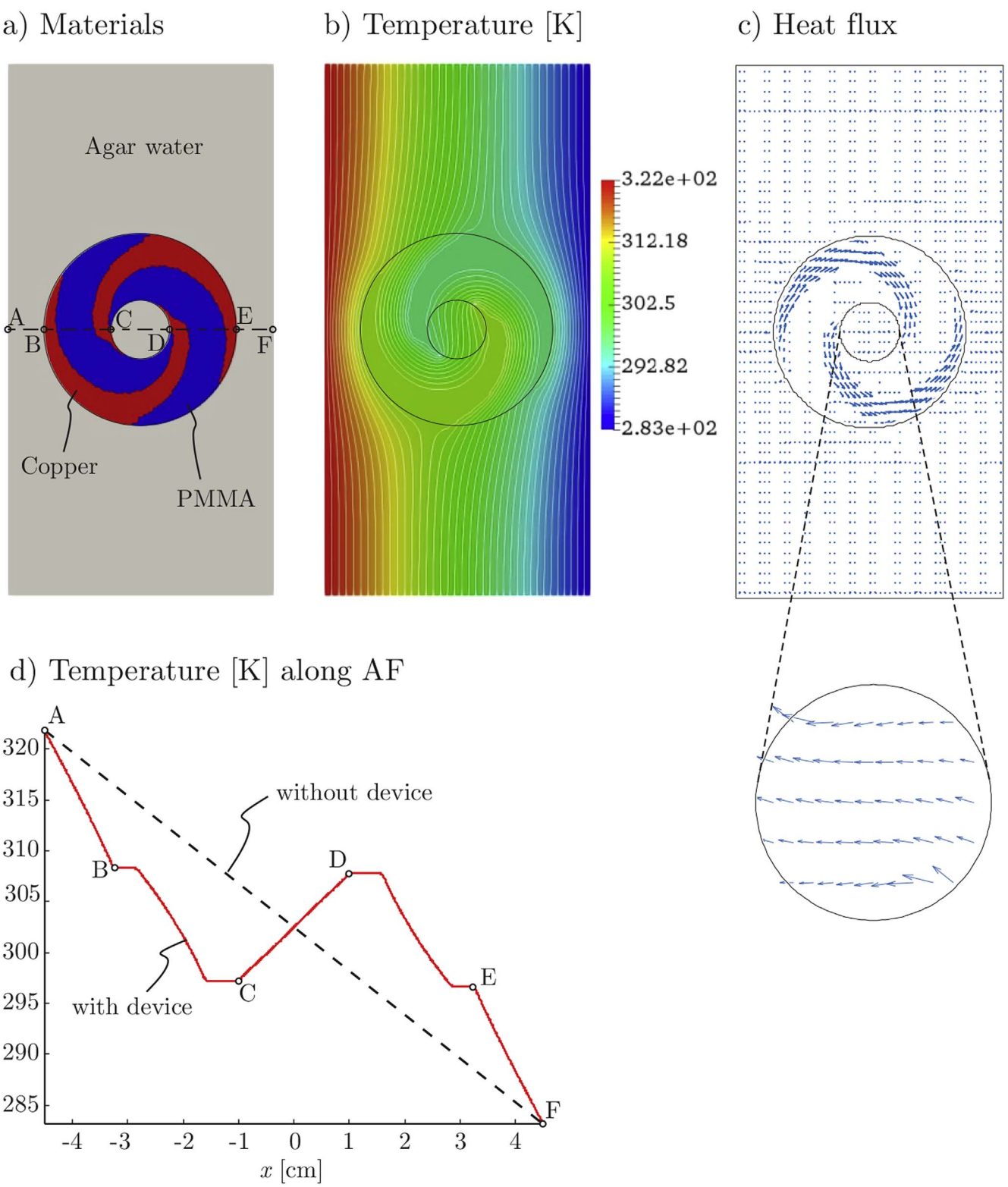

Fig. 6. Heat flux inversion device after "black-and-white" filtering of the optimal solution: a) Material distribution; b) temperature in the plate, with isotherms separated by 0.9923 K; c) heat flux in the plate, with a detail of the heat flux inside the device; d) temperature along the line AF.

exactly the same strategy as that used to solve the previously described problem for combined cloaking and inversion: IPOPT [27] is used as the optimization solver, $p = 3$ in the SIMP conductivity function (16), $\tilde{r}_{\text{filtr}} = 3.5$ mm in the density filter definition (26), and $P_e = 0.5$ as initial guess.

Fig. 4a shows the optimal solution for the copper fraction in the device, whose inclusion produces the temperature and heat flux distributions throughout the plate depicted in Fig. 4b and c; Fig. 4d shows a detail of the temperature along the central line AF.

Now, the heat inversion task was very closely accomplished: RMSE $= 0.0048 q_0$.

5.1. Using black-and-white filtering for fabricability

It is apparent from Fig. 4a that the solution is not free of "grey"

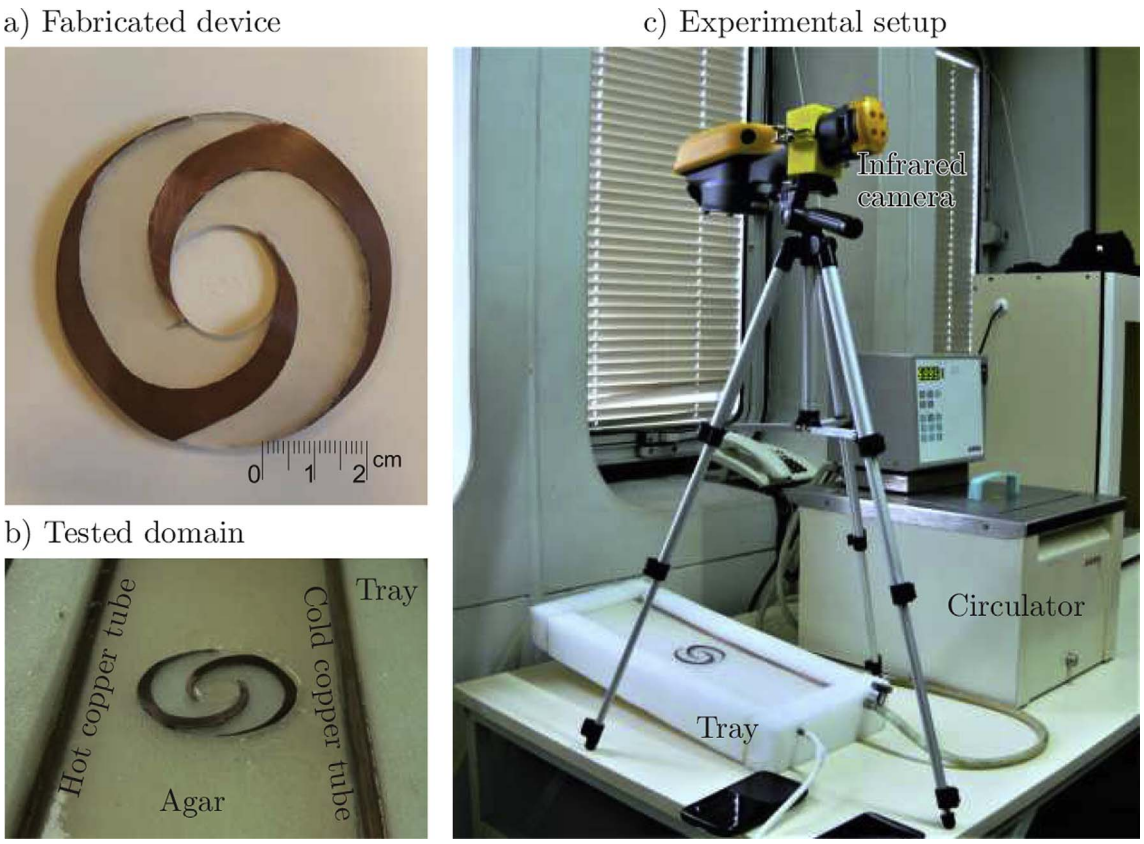

Fig. 7. Experimental heat flux inversion: a) hand-made device; b) domain of analysis; c) experimental setup.

zones, i.e. those elements where $0 < P_e < 1$ making the material be neither copper nor PMMA but a mixture of them. This complicates the fabrication of the device, which is a main concern in this work. To avoid grey zones, recourse can be made to "black-and-white" filters [24]. In this work, a simple a posteriori "black-and-white" filtering strategy is applied: if the copper fraction $w^{(e)}_{\text{copper}}$ at an element $\Omega^{(e)}$ is greater than w^*, the element is assumed to be fully made of copper; otherwise, it is assumed to be made of PMMA. After "black-and-white" filtering for different choices of w^*, the task is not as well accomplished as for the optimal solution with "grey zones" given by Fig. 4a. From Fig. 5, it is apparent that the best deal between optimality and fabricability is obtained for $w^* = 0.02$, with an error RMSE $= 0.4499 q_0$ in the heat inversion task. The corresponding material, temperature and heat flux distributions are shown in Fig. 6.

Note that the accomplishment of the heat inversion task has been considerably deteriorated when the "grey" zones are eliminated: this is the price to pay for manufacturability. Notwithstanding, considering heat flux inversion, the highly simplified device in Fig. 6a still performs better than the Narayana and Sato's one.

6. Experimental validation

In this section, we aim to highlight the easy manufacturability of the recently designed heat flux inverter and to give experimental validation to the numerically determined results.

Fig. 7a shows the experimental device fabricated following the design in Fig. 6a. It is so easy to fabricate that it could be hand-made, as it was done here. Using a jeweler's saw, the two blades of the copper helix were cut from a 4 mm-thick plate, and the two blades of the PMMA helix were cut from a 4 mm-thick plate. The cuts were done with a tolerance of $\pm$ 0.5 mm. All these parts were assembled to build the device using cyanoacrylate as adhesive, which completely filled the narrow gaps between the copper and the PMMA (that were fabrication defects). This adhesive has a conductivity of 0.2 $\text{Wm}^{-1}\text{K}^{-1}$, close to that of the PMMA; so, regarding steady heat conduction, it can be considered that the material in the interface copper/PMMA closely behaves like PMMA.

We put this device in the center of the bed of a horizontal tray, which has its bottom and walls made of 5 cm-thick sheets of expanded polyethylene (EPE), a material with very low conductivity (about 0.04 $\text{Wm}^{-1}\text{K}^{-1}$). The tray was equipped with 5 mm-diameter copper tubes along its long sides for realizing the boundary conditions. Then, a hot 3%-agar aqueous solution was poured into the tray and left to cool to 277.15 K during 12 h to build a gel. As a result, an excellent contact was obtained at the interfaces agar/device and agar/side copper tubes. Fig. 7b shows the final experimental configuration of the domain including the device embedded in agar.

To realize the boundary conditions, one of the copper tubes was connected to a close circuit with water at $T_{\text{hot}} = 303.15$ K$\pm$ 0.01 K, while the other one was connected to a close circuit with water at $T_{\text{cold}} = 283.15$ K $\pm$ 0.01 K. The temperature and flow of the hot and cold water circuits were controlled using Julabo TD-12 thermostatic circulators.

The experiment was conducted under an environmental temperature of 293.65 K $\pm$ 0.5 K, while the temperature in the tested domain at the beginning of the experiment (that is, when the circulator was turned on) was 293.15 K.

The evolution of the temperatures along the experiment was registered using a Fluke Ti100 infrared camera, which has an accuracy of $\pm$ 2 K for the temperature range of the experiment.

Fig. 7c shows the whole experimental setup.

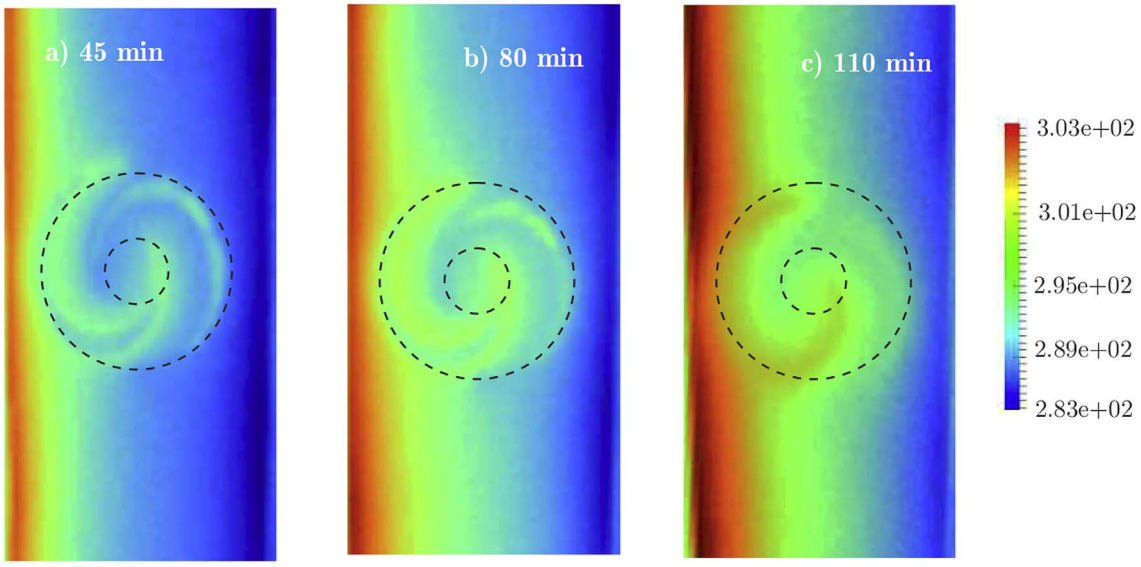

Fig. 8. Thermal images of the agar plate and the device from the infrared camera: a) 15 min; b) 45 min; and c) 110 min.

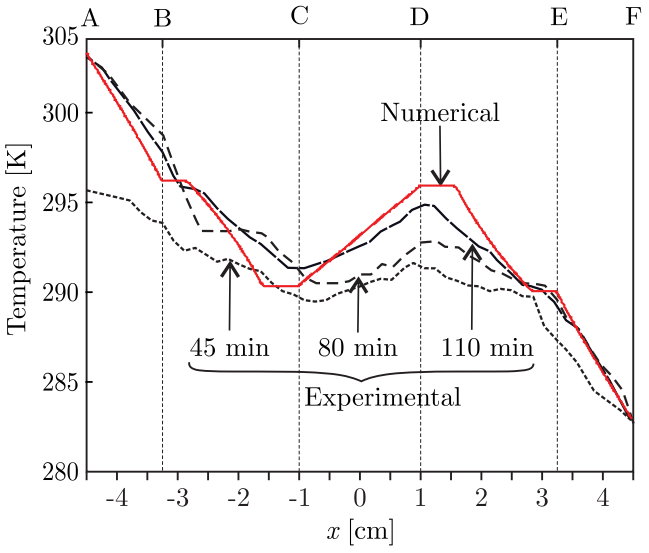

Fig. 9. Temperature along the line AF: experimental vs. numerical.

Let us remark that the current experiment reproduces the hypotheses of the numerical model (those from the Narayana and Sato's experiment [5] also) concerning the geometry of the device and the agar plate, the employed materials, and the boundary conditions, except for the prescribed temperature T_{hot} at the hot side ($x = -L_x/2$).

The original $T_{\text{hot}} = 321.85$ K from both Narayana and Sato's experiment and the current numerical model could not be used because of the melting of agar next to the hot tube. Since melting invalidates the pure heat conduction assumption, we decided to adopt $T_{\text{hot}} = 303.15K$ for the current experiment. Now, the magnitude of the heat flux in the plate without the device is $q_0 = 126.67$ Wm^{-2}, and the new temperature distribution is qualitatively identical to that shown in Fig. 6b and d, where only the upper bound of the temperature range needs to be changed. So, the ability of the current device to invert the heat flux is not affected at all by this change.

6.1. Results and discussion

The experiment timeline was assumed to start when the circulator was turned on to take the copper tubes to their prescribed temperatures. At this instant, the tested domain (that shown in Fig. 7b) was at 293.15 K. Then, the temperature evolution in the test domain was registered every five minutes. All along the experiment, the environmental temperature was 293.65 K ± 0.5 K.

After 45 min, Fig. 8a, the agar plate next to the cold tube attained its prescribed temperature T_{cold} but the hotter side was still 8 K below T_{hot}. Nevertheless, note that the heat flux inversion at the center of the plate was already developed. After 80 min, Fig. 8b, the temperature of the hotter side reached T_{hot}. After 110 min, Fig. 8c, the temperature field in the whole agar plate with the embedded device could be considered in steady state, and the heat flux was clearly inverted in the center.

This can be quantitatively assessed from the curves in Fig. 9 showing the evolution of the temperature along the central line AF during the experiment, together with the numerically computed steady temperature along this line. On the base of the experimental temperature at 110 min, an average heat flux across the central heat inversion region can be defined as

$$q_{\text{invert}} = -k_{\text{agar}} \frac{T_{\text{C}} - T_{\text{D}}}{d_{\text{inner}}} = 97.98 \text{ Wm}^{-2}. \tag{32}$$

This flux points opposite to $\mathbf{q}_0$ and its magnitude is 0.77 q_0. By doing so, the current device performs better than the inverter fabricated by Narayana and Sato [5], where the magnitude of the inverse flux was only 0.40 times the magnitude of the original flux. And, let us recall it, the current device is considerable easier to make than Narayana and Satos's one.

Further, as it can be observed in Fig. 9, there is a qualitatively good agreement between the numerical steady temperature and the experimental one at 110 min. The differences between both curves are always less than 2 K in magnitude, which is the accuracy of the infrared camera used to register the experiment.

Regarding the reverted temperature gradient in the central segment CD, that the experimental one be smaller than the numerical one can be caused by heat losses through the top surface of the experimental device, which were not accounted for the numerical model. The absence of heat transfer across the plate in the numerical model can also explain why the

plateaux observed in the numerical curve just after the points B and D and just before the points C and E are smoothed in the experimental curve.

7. Conclusions

We proposed an optimization-based method for the design of easy-to-make devices to accomplish a given, arbitrary, heat flux manipulation task. The error in accomplishing this task is the function to minimize. There is one design variable per finite element in the device, making the current nonlinear constrained optimization problem a large scale one with thousands of design variables. Each design variable defines the material at the corresponding finite element, being one of two given materials with highly different thermal conductivity.

We applied this method for designing a device for heat flux inversion, which is an extreme heat flux guidance task. The so-designed device was very easy to fabricate, enabling us to reproduce it by hand-cutting. An experiment was then conducted to prove the efficiency of this device for heat flux inversion, founding that it performed better than a sensibly more complicated device, that of Narayana and Sato [5], that was usually taken as example of the extreme heat flux manipulation.

By making so easy to manipulate the heat flux, this work paves the way to practical applications, which will be the goal of our future works.

Acknowledgements

We thank the following institutions for supporting this work:

• The European Research Council (ERC), through the project "Advanced Tools for Computational Design of Engineering Materials (COMP-DES-MAT)" (FP/2007–2013, ERC Grant Agreement 320815).

• The Argentine Agency for Scientific and Technological Promotion (ANPCyT), through the project "Computational Design of Metamaterials" (PICT-2016-2673).

• The National Littoral University (UNL) at Santa Fe, Argentina, through the project "Metamaterials: Computational Design, Thermal, Mechanical and Acoustic Applications, and Prototyping" (CAI + D 2016 087LI).

Appendix. Applications to concentration and shielding

The current approach is able to accommodate different heat flux manipulation tasks using the same objective function. So, the objective functions for cloaking, inversion, concentration and shielding (as well as any other task where the heat flux has to take prescribed values at a series of points) have the same units and can be easily combined (using the classical weighted sum method [30], for instance). This is a crucial advantage with respect to the optimization-based approach for heat flux manipulation proposed by Dede et al. [7], where the objective functions for concentration and shielding have units of heat flux per length while that for inversion is the weighted sum of two terms with yet different units (heat flux and square heat flux).

In this appendix, we show applications of the current approach to heat concentration and shielding. In all the cases along this paper, including the current ones, the objective function is that given by equation (15) with $\overline{\mathbf{q}}^{(q)} = \alpha \mathbf{q}_0$, where $\mathbf{q}_0$ is the external given heat flux, and $\alpha = -1$ for the elements in the inversion region, $\alpha = 1$ for those in the cloaking region, $\alpha = 0$ for those in the region to be shielded, and $\alpha > 1$ for those in the region of heat concentration.

For the current problems, the domain and the boundary conditions are those shown in Fig. 2, where Ω_{invert} (the region enclosed by the device) now denotes either the concentration or the shielding region. In Ω_{cloak}, i.e. outside the device, no task is prescribed.

Being the current problems mathematically identical to those solved in Sections 4 and 5, they were solved using exactly the same strategy: IPOPT [27] is the optimization solver, $p = 3$ in the SIMP conductivity function (16), $\tilde{r}_{\text{filtr}} = 3.5$ mm in the density filter definition (26), and $P_e = 0.5$ as initial guess.

The solution for the concentration problem with $\alpha = d_{\text{outer}}/d_{\text{inner}} = 3.125$ gives the material distribution shown in Fig. 10a, which produces the temperature distribution shown in Fig. 10b. For this solution, the error in the accomplishment of the concentration task (objective function) is RMSE $= 0.67 q_0 = 0.21 \alpha q_0$, and the average heat flux over all the finite elements enclosed by the device is $[2.63 \;\; 0.00]^T q_0$.

For the shielding problem, the solution determines the material distribution shown in Fig. 11a, causing the temperature distribution in Fig. 11b. For this solution, the objective function takes the value RMSE $= 0.0003 q_0$, and the average heat flux over all the finite elements enclosed by the device is $[0.07 \;\; 0.00]^T q_0$.

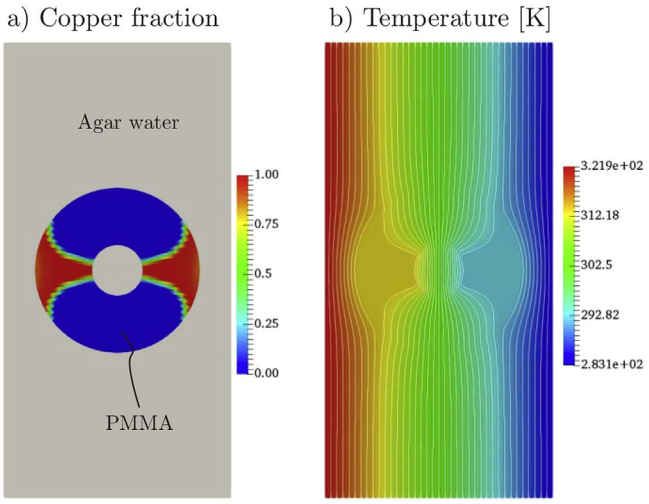

Fig. 10. Optimal solution for the heat concentration device: a) Fraction of copper in the device; b) temperature in the plate, with isotherms separated by 0.9923 K.

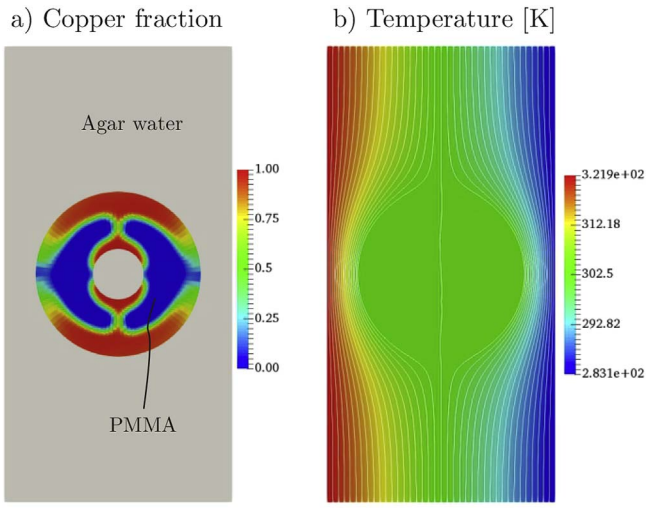

Fig. 11. Optimal solution for the heat shielding device: a) Fraction of copper in the device; b) temperature in the plate, with isotherms separated by 0.9923 K.

References

[1] M. Maldovan, Sound and heat revolutions in phononics, Nature 503 (2013) 209–217.
[2] M. Kadic, T. Bückmann, R. Schittny, M. Wegener, Metamaterials beyond electromagnetism, Rep Prog Phys 76 (2013) 126501.
[3] F. Chen, D.Y. Lei, Experimental realization of extreme heat flux concentration with easy-to-make thermal metamaterials, Sci Rep 5 (2015) 11552.
[4] C.Z. Fan, Y. Gao, J.P. Huang, Shaped graded materials with an apparent negative thermal conductivity, Appl Phys Lett 92 (2008) 251907.
[5] S. Narayana, Y. Sato, Heat flux manipulation with engineered thermal materials, Phys Rev Lett 108 (2012) 214303–214308.
[6] E.M. Dede, T. Nomura, P. Schmalenberg, J.S. Lee, Heat flux cloaking, focusing, and reversal in ultra-thin composites considering conduction-convection effects, Appl Phys Lett 103 (2013) 063501.
[7] E.M. Dede, T. Nomura, J. Lee, Thermal-composite design optimization for heat flux shielding, focusing, and reversal, Struct Multidiscip Optim 49 (2014) 59–68.
[8] S. Narayana, S. Savo, Y. Sato, Transient heat flux shielding using thermal metamaterials, Appl Phys Lett 102 (2013) 201904.
[9] R. Schittny, M. Kadic, S. Guenneau, M. Wegener, Experiments on transformation thermodynamics: molding the flow of heat, Phys Rev Lett 110–19590 (2013) 1–5.
[10] V.D. Fachinotti, I. Peralta, A.E. Huespe, A.A. Ciarbonetti, Control of heat flux using computationally designed metamaterials, 5th international conference on engineering optimization (EngOPT2016), Iguasscu Falls, Brasil, 19-23 June, 2016, p. 7.
[11] I. Peralta, V.D. Fachinotti, A.A. Ciarbonetti, Optimization-based design of a heat flux concentrator, Sci Rep 7 (2017) 40591.
[12] J.B. Pendry, D. Schurig, D.R. Smith, Controlling electromagnetic fields, Science 312 (5781) (2006) 1780–1782.
[13] E.M. Dede, Simulation and optimization of heat flow via anisotropic material thermal conductivity, Comput Mater Sci 50 (2010) 510–515.
[14] K.P. Vemuri, F.M. Canbazoglu, P.R. Bandaru, Guiding conductive heat flux through thermal metamaterials, Appl Phys Lett 105 (2014) 193904.
[15] M.P. Bendsøe, O. Sigmund, Topology optimization. Theory, methods, and applications, Springer-Verlag, 2003.
[16] J. Dirker, J.P. Meyer, Topology optimization for an internal heat-conduction cooling scheme in a square domain for high heat flux applications, ASME Journal of Heat Transfer 135 (2013) 111010.
[17] O. Puigdellivol, D. Méresse, Y. Le Menach, S. Harmand, J. Wecxsteen, Thermal topology optimization of a three-layer laminated busbar for power converters, IEEE Trans Power Electron 32 (6) (2017) 4691–4699.
[18] O.C. Zienkiewicz, R.L. Taylor, The finite element method, Vol. 1: the basis, Butterworth-Heinemann, 2000.
[19] E. Lund, J. Stegmann, On structural optimization of composite shell structures using a discrete constitutive parametrization, Wind Energy 8 (1) (2005) 109–124.
[20] M. Kachanov, I. Sevostianov, On quantitative characterization of microstructures and effective properties, Int J Solid Struct 42 (2005) 309–336.
[21] I. Tsukrov, M. Kachanov, Effective moduli of an anisotropic material with elliptical holes of arbitrary orientational distribution, Int J Solid Struct 37 (2000) 5919–5941.
[22] C. Rungsiyakull, Q. Li, G. Sun, W. Li, M.V. Swain, Surface morphology optimization for osseointegration of coated implants, Biomaterials 31 (2010) 7196–7204.
[23] J. Chen, C. Rungsiyakull, W. Li, Y. Chen, M. Swain, Q. Li, Multiscale design of surface morphological gradient for osseointegration, J. Mech. Behav. Biomed. Mater. 20 (2013) 387–397.
[24] O. Sigmund, Morphology-based black and white filters for topology optimization, Struct Multidiscip Optim 33 (2007) 401–424.
[25] D.A. Tortorelli, P. Michaleris, Design sensitivity analysis: overview and review, Inverse Probl Eng 1 (1) (1994) 71–105.
[26] H. Chen, C.T. Chan, Transformation media that rotate electromagnetic fields, Appl Phys Lett 90 (2007) 241105.
[27] A. Wächter, L.T. Biegler, On the implementation of an interior-point filter line-search algorithm for large-scale nonlinear programming, Math. Program., Ser. A 106 (2006) 25–57.
[28] J.W. Eaton, D. Bateman, S. Hauberg, R. Wehbring, GNU Octave version 4.0.3 manual: a high-level interactive language for numerical computations, (2016) URL http://www.gnu.org/software/octave/doc/interpreter.
[29] J. Nocedal, S.J. Wright, Numerical optimization, second ed., Springer, 2006.
[30] R.T. Marler, J.S. Arora, The weighted sum method for multi-objective optimization: new insights, Struct Multidiscip Optim 41 (2010) 853–862.